Earth, Planets and Space

TECHNICAL REPORT

Identification of marine magnetic anomalies based on the sliding window curve similarity method

Mingming Wang[1,2,3*], Jing Cao[1], Jianlou Li[1] and Xianghong Liu[1]

Abstract: Marine magnetic anomalies play an essential role in plate tectonics and geodynamics. The conventional method to identify marine magnetic anomalies is to visually compare synthetic and observed magnetic anomaly profiles, and there is usually no quantitative evaluation for the identification results. Therefore, we developed the sliding window curve similarity (SWCS) method to objectively identify marine magnetic anomalies and quantitatively evaluate the identification results. The synthetic model tests and practical applications show that the SWCS method is feasible and effective in identifying fast-spreading marine magnetic anomalies. The applications of the SWCS method show that the theoretical windows using combined polarity chrons can improve the accuracy of identification.

Keywords: Marine magnetic anomalies, Objective identification, Quantitative evaluation, Sliding window curve similarity

Graphical Abstract

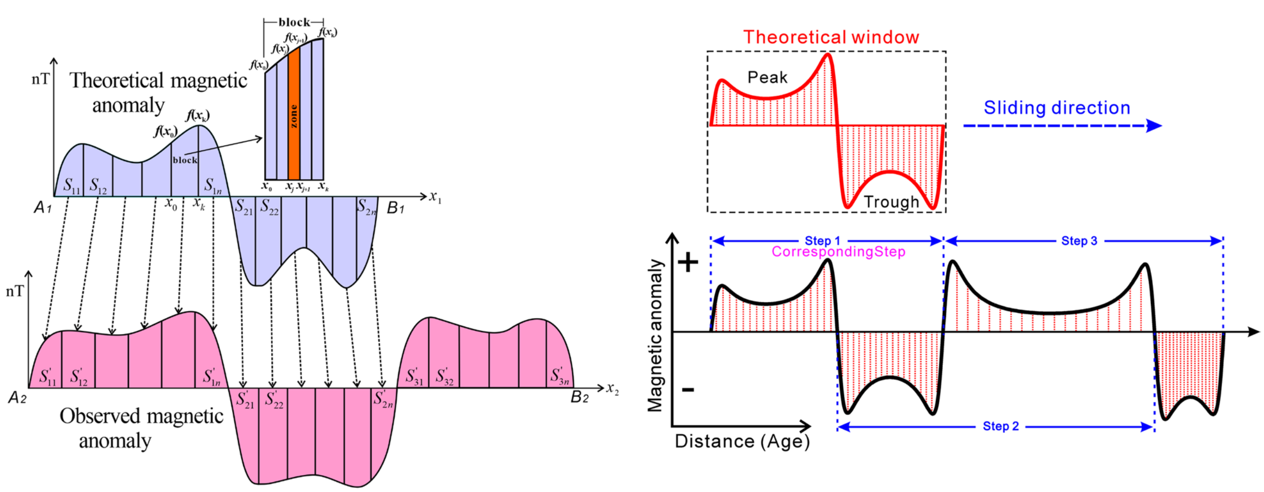

*Correspondence: wmm@ahszu.edu.cn
[1] School of Resources and Civil Engineering, Suzhou University, Suzhou 234000, China
Full list of author information is available at the end of the article

Introduction

Marine magnetic anomalies cover large areas of oceanic basins and provide strong evidence for the seafloor spreading process (Vine and Matthews, 1963). Marine magnetic anomalies are caused by thermoremanent magnetization of the oceanic crust and record the palaeomagnetic field when magma rises at spreading ridges and cools below the Curie temperature (Vine, 1966; Dyment and Arkani-Hamed, 1995). The interpretation of marine magnetic anomalies is of great significance in plate tectonics and geodynamics (e.g., Vine and Matthews, 1963; Harrison, 1987; Veevers and Li, 1991; Gee and Kent, 2007; Müller et al., 2008; Granot and Dyment, 2015; Wang and Liu, 2018; Choe and Dyment, 2020; Tominaga et al., 2021; Li et al., 2021; Gürer et al., 2022). The conventional method of identifying marine magnetic anomalies is to visually compare synthetic and observed magnetic anomaly profiles (Harrison, 1987; Gee and Kent, 2007; Jacob et al., 2014). The identification results much depend on the experience of experts and rarely provide a quantitative evaluation. Honsho et al. (2009) attempted to calculate the coherency between the modelled and observed magnetic anomalies in the spectral domain to provide an evaluation of the visually identified results. However, the coherency is limited to an overall evaluation and could not provide a detailed comparison for magnetic anomalies of different polarity chrons.

Here we propose the sliding window curve similarity (SWCS) to objectively identify marine magnetic anomalies and quantitatively evaluate the identification results. First, the SWCS method is introduced, and then marine magnetic anomalies are simulated by synthetic models to test the feasibility and robustness of the SWCS method. Last, the SWCS method is applied to the observed marine magnetic anomalies in the Pacific Ocean.

Sliding window curve similarity method

Curve similarity of marine magnetic anomalies

The visual identification process of marine magnetic anomalies is equivalent to comparing the curve similarity between the synthetic and observed magnetic anomalies. To realize a similar identification process by the computer, it is necessary to find the quantitative parameter which can reflect the shape of the marine magnetic anomalies. Therefore, the concept of the curve similarity of marine magnetic anomalies is proposed here. The

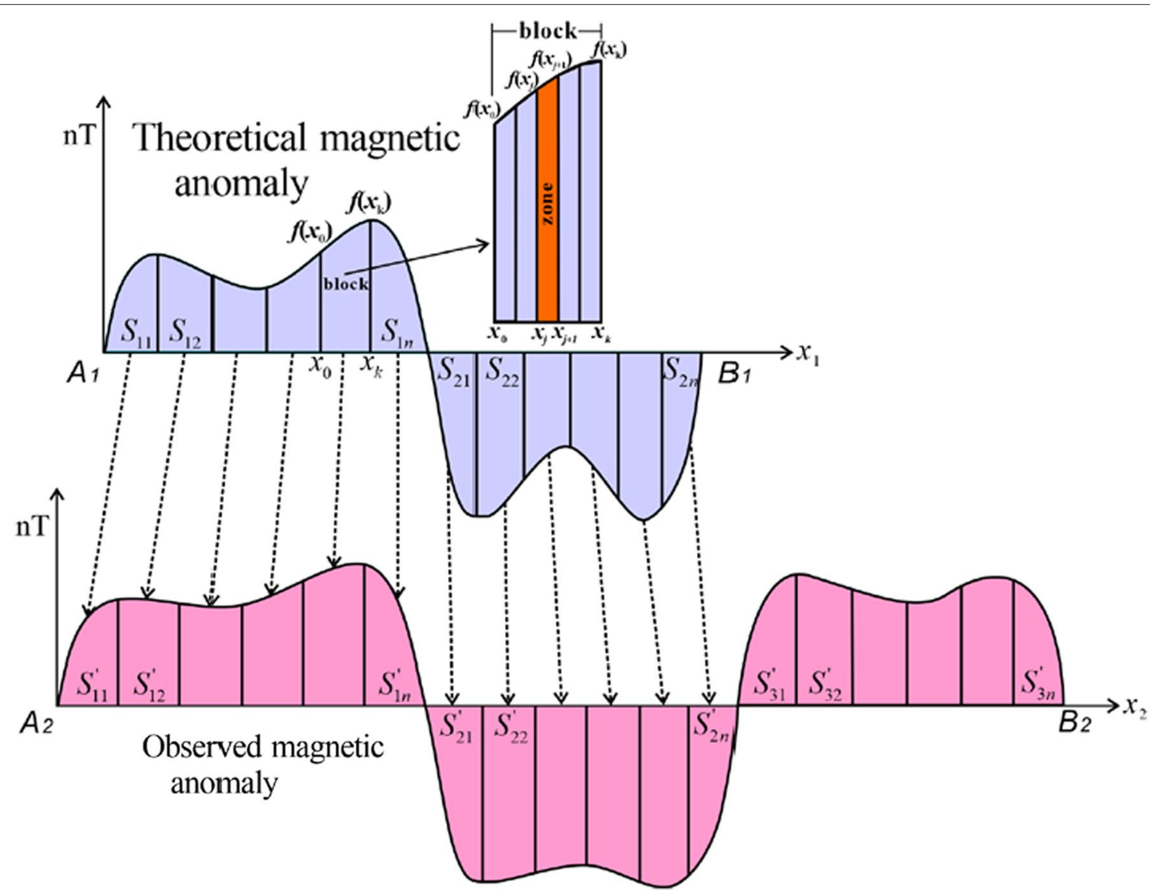

Fig. 1 The diagram of subdivision of the synthetic and observed marine magnetic anomalies

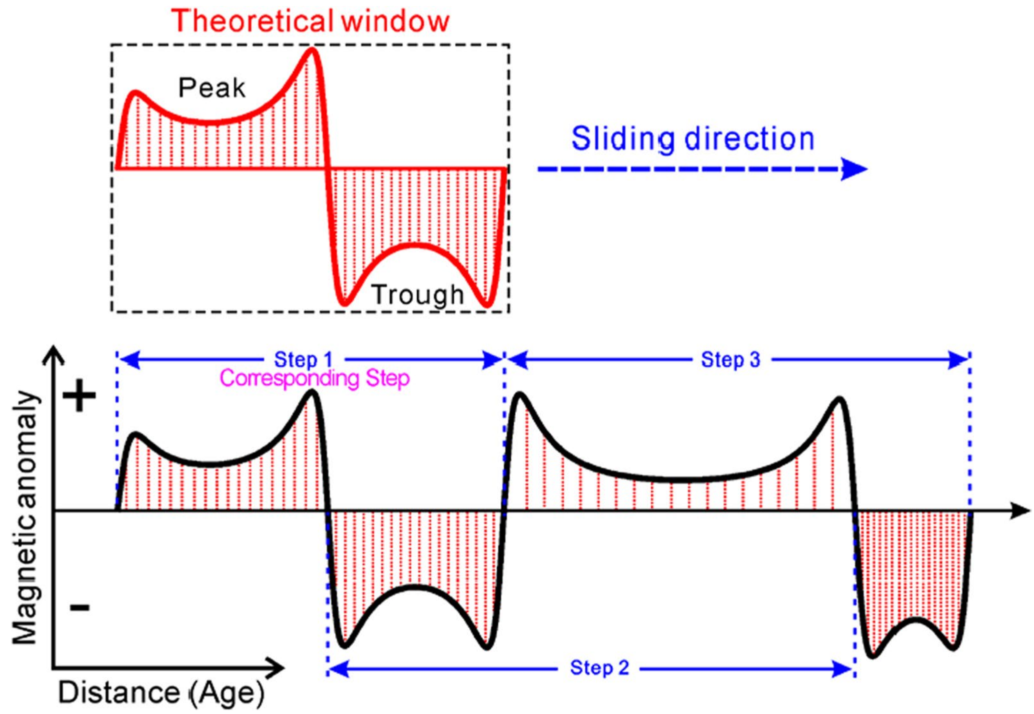

Fig. 2 The schematic diagram of the sliding window technique

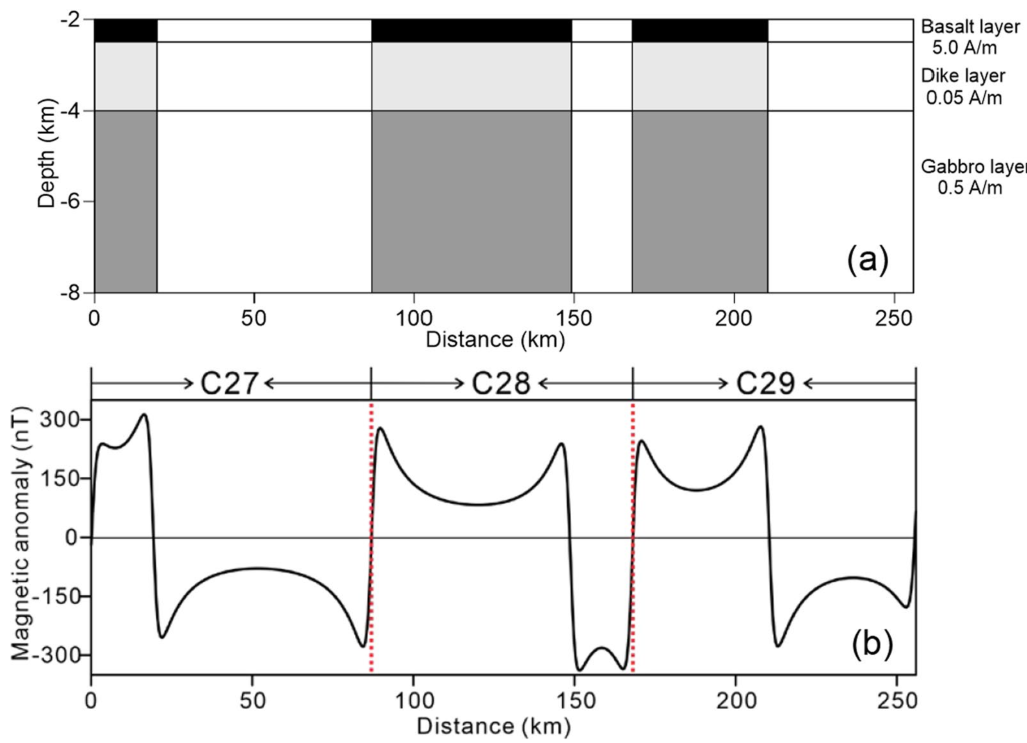

Fig. 3 The three-layer oceanic crust model and forward modelled marine magnetic anomalies. **a** Schematic diagram of the three-layer oceanic crust model. **b** The forward modelled marine magnetic anomalies of the three-layer oceanic crust model. Red dashed lines show the boundaries for different polarity chrons from C27 to C29

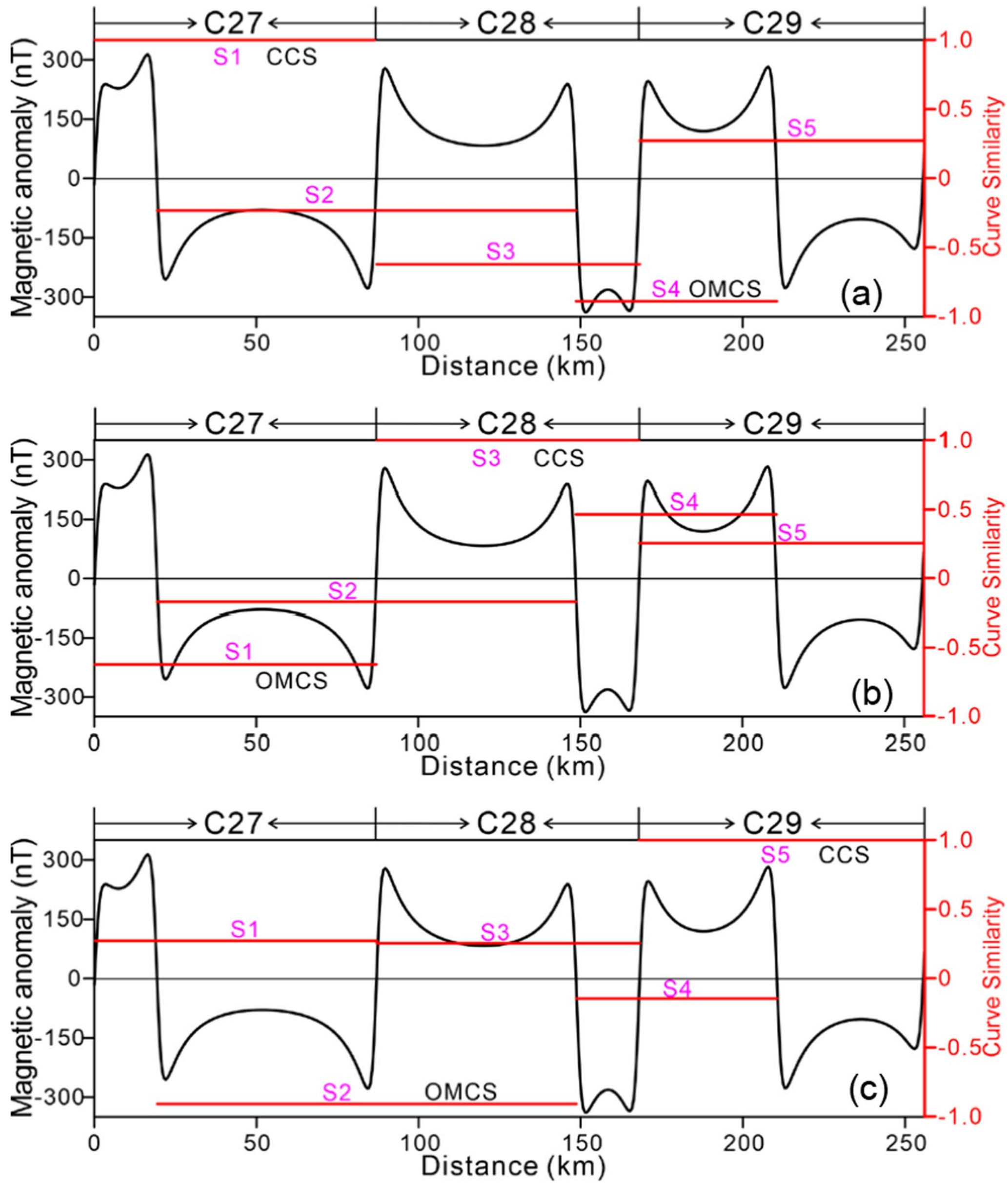

Fig. 4 Identification results of magnetic anomalies of polarity chron C27-29 by the SWCS method. **a** The identification results of polarity chron C27. **b** The identification results ofpolarity chron C28. **c** The identification results of polarity chron C29. The red lines represent the values of the curve similarity in different steps (Magenta marks). The CCS represents the curve similarity between the theoretical window and the observed magnetic anomalies at the position of the corresponding steps. The OMCS represents the maximum absolute curve similarity values between the theoretical window and the observed magnetic anomalies at the position outside of the corresponding steps

definition of the curve similarity of marine magnetic anomalies is as follows.

First, assume that the synthetic magnetic anomaly curve is A_1B_1 and the observed magnetic anomaly curve is A_2B_2 (Fig. 1). Every peak and trough of the curve A_1B_1 and A_2B_2 is divided into *n* blocks, and then each block is divided into *k* small zones. Second, integrate the small zones within each block to calculate the areas of each block by *Eq.* 1.

$$S_{block} = \int_{x_0}^{x_k} f(x)dx = \sum_{j=0}^{k-1} \frac{1}{2}\left[f(x_j) + f(x_{j+1})\right] \cdot (x_{j+1} - x_j) \quad (1)$$

The block area set of every peak and trough of the synthetic magnetic anomalies is denoted by $P_s = \{S_{p1}, S_{p2}, ..., S_{pn}\}$, and the block area set of every peak and trough of the observed magnetic anomalies is denoted by $Q_s = \{S_{q1}, S_{q2}, ..., S_{qn}\}$.The similarity between the peaks (troughs) of synthetic magnetic anomalies and peaks (troughs) of the observed magnetic anomalies are calculated by the adjusted cosine similarity as *Eq. 2*.

$$Sim = \frac{(P_s - \overline{p}) \cdot (Q_s - \overline{q})}{|P_s - \overline{p}||Q_s - \overline{q}|} = \frac{\sum_{i=1}^{n} (S_{p_i} - \overline{p})(S_{q_i} - \overline{q})}{\sqrt{\sum_{i=1}^{n} (S_{p_i} - \overline{p})^2}\sqrt{\sum_{i=1}^{n} (S_{q_i} - \overline{q})^2}} \quad (2)$$

where $\overline{p}, \overline{q}$ are the mean value of the P_s *and* Q_s, respectively.

The sliding window technique

The sliding window technique automatically calculates the curve similarities between the synthetic and observed magnetic anomalies. First, the synthetic magnetic anomalies are modleled based on the geomagnetic polarity timescale (e.g., Cande and Kent, 1995). Then the synthetic magnetic anomalies are divided into fragments as theoretical windows. Last, make these theoretical windows slide along the observed magnetic anomaly profile to calculate the curve similarity between peaks and troughs of the synthetic and observed magnetic anomalies (Fig. 2). If the theoretical window includes not only one peak or trough, the average curve similarity of peaks and troughs is used. Every peak and trough of the synthetic and observed magnetic anomalies are divided into n blocks, and then make the theoretical window slides along the observed magnetic anomaly profile with a step length of n blocks. Thus, the peaks and troughs of the theoretical window can correspond to the peaks (troughs) and troughs (peaks) of the observed magnetic anomalies. Curve similarity values will be calculated in different sliding steps when the theoretical window is sliding along the observed magnetic anomaly profile. The curve similarity will be the highest when the theoretical window slides overlap the corresponding step. Thus, the marine magnetic anomalies are identified.

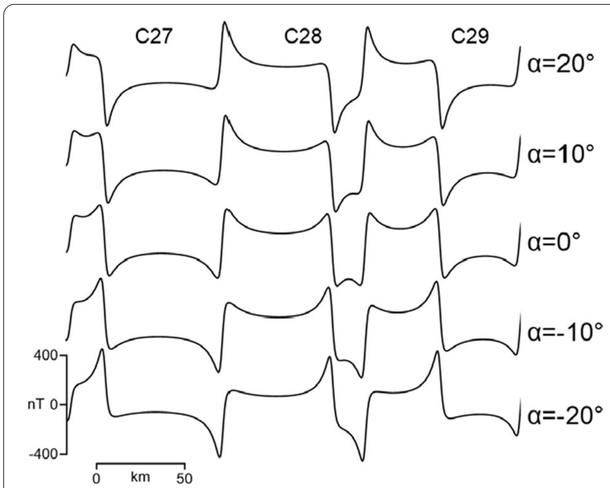

Fig. 5 Magnetic anomalies of polarity chron C27, C28 and C29 with different skewness

Synthetic marine magnetic anomaly test

Synthetic marine magnetic anomaly model

The single-layer model with the 0.5 km thick basalt layer to forward model marine magnetic anomalies is widely used in marine magnetic anomalies interpretation (e.g.,Vine and Matthews, 1963; Korenaga, 1995; Roberts and Lewin-Harris, 2000; Li et al., 2014, 2018). However, the magnetic anomalies induced by the dike and gabbro layers are also significant components of the marine magnetic anomaly (e.g., Cande and Kent, 1976; Blakely, 1976; Kidd, 1977; Dyment et al., 1994; Dyment and Arkani-Hamed, 1998; Gee and Kent, 2007; Granot and Dyment, 2019). Therefore, we modelled the marine magnetic anomalies by a three-layer oceanic crust model. The seafloor is at 2.0 km depth, the uppermost is the basalt layer with 5.0 A/m magnetization and 0.5 km thick, the second layer is the dike layer with 0.05 A/m magnetization and 1.5 km thick, the third layer is the gabbro layer with 0.5 A/m magnetization and 4.0 km thick. As a standard reference for comparison, the boundaries of normal and reversed magnetized blocks in each magnetic layer are assumed to be vertical (Fig. 3a). The directions of the geomagnetic field and magnetization are assumed to be vertical. The time of the marine magnetic anomalies is 60.9 Ma ~ 65.5 Ma from polarity chron C27 to C29. The magnetization distribution is based on the CK95 geomagnetic polarity time scale (Cande and Kent, 1995). The full spreading rate of the marine magnetic anomalies is 110 mmyr^{-1}. The method to calculate the magnetic anomalies of polygonal blocks was first proposed by Talwani (1964), and then Won and Bevis (1987) improved the algorithm. Here, we use the method of Won and Bevis (1987) to calculate the magnetic anomalies. Figure 3b shows the forward modelled marine magnetic anomalies based on the three-layer oceanic crust model.

To show the identification process and verify the correctness of the algorithm, the forward modelled marine magnetic anomalies (Fig. 3b) are divided into three fragments, C27, C28 and C29, as theoretical windows. The

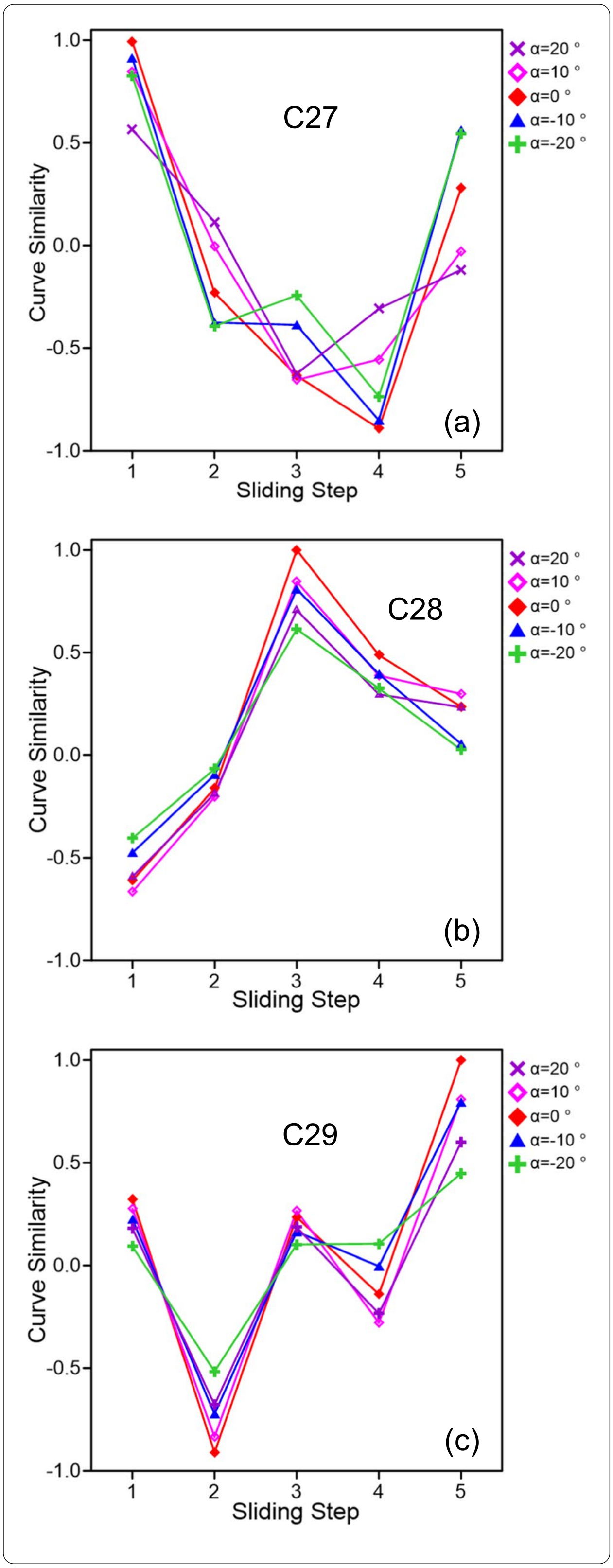

Fig. 6 Identification results of the polarity chron C27, C28 and C29 under different skewness of − 20°, − 10°, 0°, 10°, 20°. **a** The identification results of the polarity chron C27; **b** The identification results of the polarity chron C28; **c** The identification results of the polarity chron C29

whole magnetic anomaly profile (Fig. 3b) is treated as the observed magnetic anomalies in the following. Then make the theoretical windows slide along the observed magnetic anomaly profile by the sliding window technique to calculate the curve similarity between the synthetic and observed magnetic anomalies. In the curve similarity calculation, every peak and trough of the synthetic and observed magnetic anomalies are divided into ten blocks. Figure 4a–c show the identification results of polarity chron C27, C28 and C29 in different sliding steps. We can see that the magnetic anomalies of polarity chron C27, C28 and C29 are correctly identified at sliding steps 1, 3 and 5, respectively, with the highest curve similarity values of 1.0. Thus, the algorithm of the SWCS method is verified. In the following, we denote the curve similarity between the theoretical window and the observed magnetic anomalies as CCS when the theoretical windows slide over the corresponding step. The maximum absolute curve similarity at the position outside the corresponding steps is denoted as OMCS (Fig. 4a–c).

Identification under different skewness

Several reasons have been proposed to explain the anomalous skewness between the synthetic and observed marine magnetic anomalies, including temporal variations of the paleomagnetic field intensity, tectonic rotation of the magnetic layer, acquisition of a secondary magnetization of the basalt layer, and the sloping magnetic boundary in the deep crust and uppermost mantle (Dyment et al., 1994; Dyment and Arkani-Hamed, 1995; Gee and Kent, 2007; Ferré et al., 2021). To investigate the effects of different skewness on the identification of marine magnetic anomalies, we change the effective inclinations of total magnetization of the forward model to simulate marine magnetic anomalies with different skewness α. Figure 5 shows the forward modeled marine magnetic anomalies with skewness α of − 20°, − 10°, 0°, 10°and 20°, respectively.

The identification results of polarity chron C27, C28 and C29 are shown in Fig. 6a–c, respectively. The theoretical windows of magnetic anomalies of polarity chron C27, C28 and C29 are derived from Fig. 3b. The polarity chron C27, C28 and C29 should be identified with

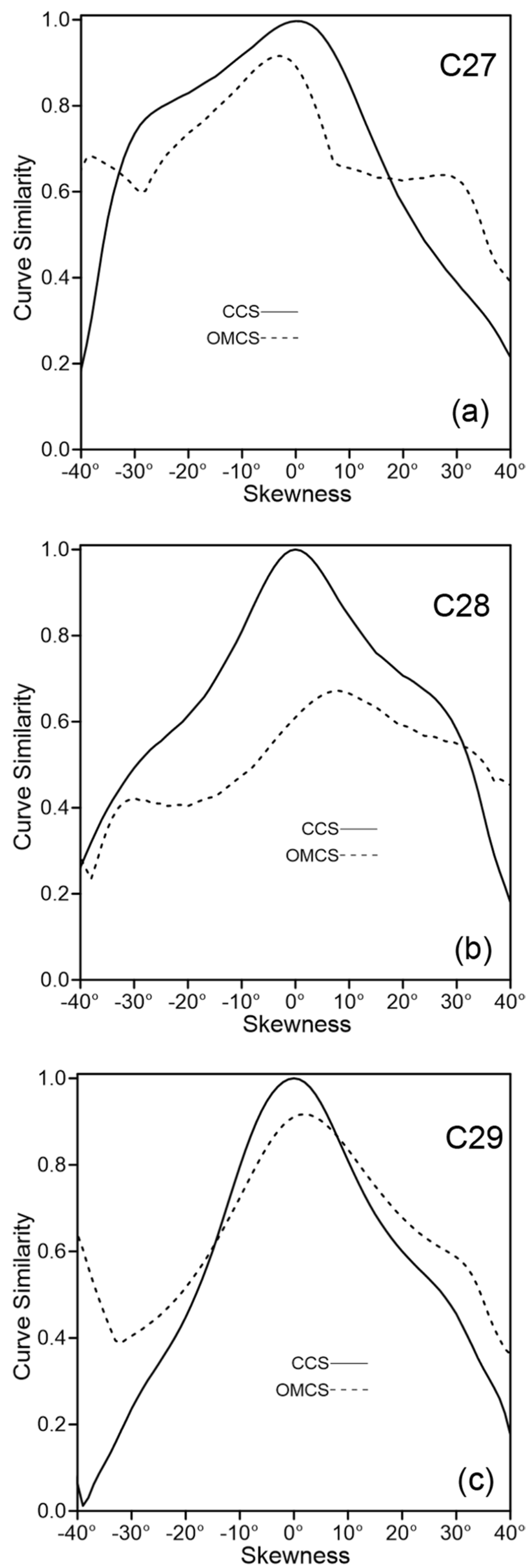

Fig. 7 The identification results of the polarity chron C27, C28 and C29 under skewness of − 40° ~ 40°. **a** The identification results of the polarity chron C27; **b** The identification results of the polarity chron C28; **c** The identification results of the polarity chron C29. The solid lines represent the curve similarity between the theoretical window and the observed magnetic anomalies at the position of the corresponding steps (CCS). The dashed lines represent the maximum absolute curve similarity values between the theoretical window and the observed magnetic anomalies at the position outside of the corresponding steps (OMCS)

the highest curve similarities at the sliding step 1, 3 and 5, respectively. The identification results show that the polarity chron C27, C28 and C29 are identified with the highest curve similarities at the corresponding sliding steps 1, 3 and 5 for skewness 20°, 10°, 0°, − 10°and − 20°. However, for polarity chron C27, the curve similarity is 0.57 at step 1 and − 0.63 at step 3 when the skewness equals 20°, the absolute curve similarity value at step 3 is greater than the curve similarity value at step1. Thus the magnetic anomaly of polarity chron C27 has the danger of misidentification when it is not clear whether the magnetic anomaly formed in the southern or northern hemisphere. The same situation exists for polarity chron C29, the curve similarity is 0.45 at step 5 and − 0.51 at step 2 when the skewness equals − 20°, and the curve similarity is 0.6 at step 5 and − 0.67 at step 2 when the skewness equals 20°.

Therefore, to investigate the detailed effects of different skewness on identifying marine magnetic anomalies, we test the skewness change from − 40°to 40°. The curve similarities between the theoretical windows and the magnetic anomaly profiles with different skewness are shown in Fig. 7a–c. The solid lines represent the curve similarity between the theoretical window and the observed magnetic anomalies at the position of the corresponding steps (CCS); for example, the corresponding steps of polarity chron C27, C28 and C29 correspond to steps 1, 3 and 5 (Fig. 4), respectively. The dashed lines represent the maximum absolute curve similarity values between the theoretical window and the observed magnetic anomalies at the position outside of the corresponding steps (OMCS). Therefore, when the CCS is greater than the OMCS, the magnetic anomalies of polarity chrons are correctly identified. The identification results show that the polarity chron C27, C28 and C29 can be correctly identified with the anomalous skewness in the range of -33° ~ 17°, -39° ~ 31° and -14° ~ 8°, respectively.

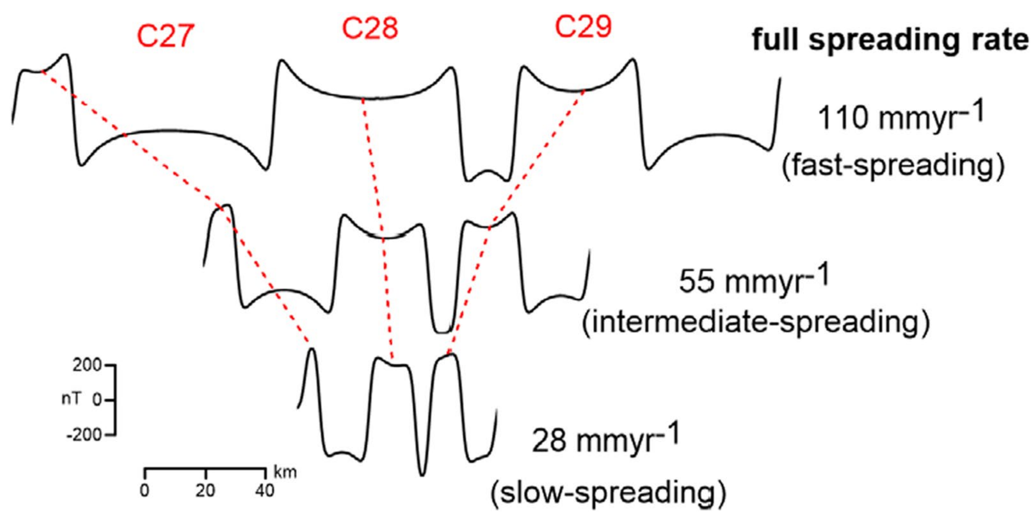

Fig. 8 Marine magnetic anomalies of the polarity chron C27-29 with different spreading rates

Identification under different spreading rates

The full spreading rates of the mid-ocean ridge can be basically divided into fast (>90 mmyr^{-1}), intermediate (50 ~ 90 mmyr^{-1}) and slow (<50 mmyr^{-1}) spreading types (Menard, 1967; Lonsdale, 1977; Macdonald, 1982; Dick et al., 2003). Figure 8 shows the magnetic anomalies of polarity chron C27 ~ C29 with fast (110 mmyr^{-1}), intermediate (55 mmyr^{-1}) and slow-spreading rates (28 mmyr^{-1}) by changing the spreading rate of the forward model in Fig. 3. We can see that the fast-spreading magnetic anomalies show a clear saddle shape for every peak and trough. As the spreading rates decreased, the saddle shape weakened and disappeared, especially for narrow anomalies. This is because the ratio of the seafloor depth to the width of the magnetization blocks increases as the spreading rate decreases. The signal attenuation significantly smooths the shape of the marine magnetic anomalies. Here, we only consider the effects of signal attenuation on the shape of the marine magnetic anomalies; spreading rates can also affect the magnetic structure of the lower crust and uppermost mantle, especially for the slowing spreading oceanic crust (see Dyment and Arkani-Hamed, 1995, for a review).

The identification results of the polarity chron C27, C28 and C29 under different spreading rates of 110 mmyr^{-1}, 55 mmyr^{-1} and 28 mmyr^{-1} are shown in Fig. 9a–c. The theoretical windows of magnetic anomalies of polarity chron C27, C28 and C29 are derived from Fig. 3b. Theoretically, the polarity chron C27, C28 and C29 should be identified with the highest curve similarities at the sliding step 1, 3 and 5, respectively. The results show that the polarity chron C27 are correctly identified with the highest curve similarities at sliding step 1 for fast-spreading (110 mmyr^{-1}) and intermediate-spreading (55 mmyr^{-1}) magnetic anomalies and failed to be identified for slow-spreading (28 mmyr^{-1}) magnetic anomalies (Fig. 9a). The polarity chron C28 are correctly identified with the highest curve similarities at sliding step 3 for fast-spreading (110 mmyr^{-1}) and intermediate-spreading (55 mmyr^{-1}) magnetic anomalies and failed to be identified for slow-spreading (28 mmyr^{-1}) magnetic anomalies (Fig. 9b). The polarity chron C29 are only correctly identified with the highest curve similarity for fast-spreading (110 mmyr^{-1}) at sliding step 5 (Fig. 9c). For slow-spreading (28 mmyr^{-1}) magnetic anomalies, the polarity chron C27, C28 and C29 are failed to be identified at the corresponding steps.

We change the spreading rates from 10 mmyr^{-1} to 200 mmyr^{-1} to investigate the detailed effects of different spreading rates on identifying marine magnetic anomalies. The curve similarities between the theoretical windows and the magnetic anomaly profiles with different spreading rates are shown in Fig. 10a–c. The identification results show that the polarity chron C27, C28 and C29 can be correctly identified with the spreading rates in the range of 38 ~ 200 mmyr^{-1}, 44 ~ 200 mmyr^{-1} and 87 ~ 200 mmyr^{-1}, respectively. Therefore, the polarity chron C27-C29 can be correctly identified under fast-spreading rates but failed to be identified at slow-spreading rates.

Identification under random noises

The geomagnetic field is dynamic and constantly changing (Gee et al., 2000; Busse and Simitev, 2008; Laj and

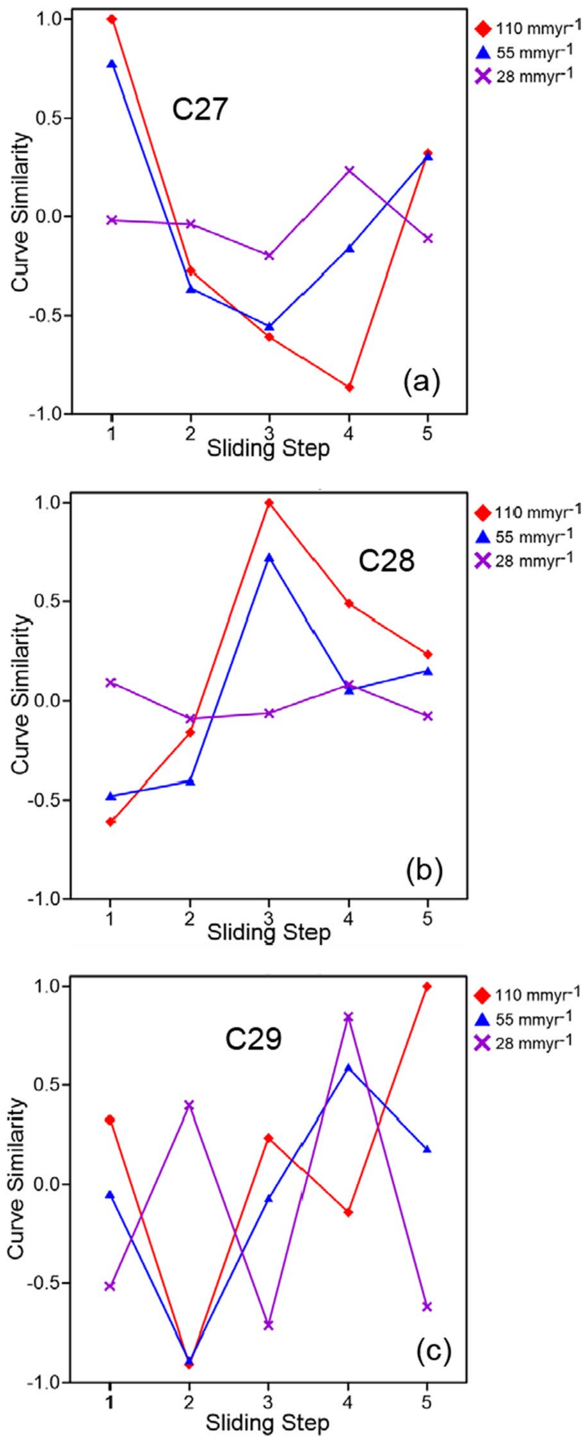

Fig. 9 Identification results of the polarity chron C27, C28 and C29 under different spreading rates of 110 $mmyr^{-1}$, 55 $mmyr^{-1}$ and 28 $mmyr^{-1}$. **a** The identification results of the polarity chron C27; **b** The identification results of the polarity chron C28; **c** The identification results of the polarity chron C29

Channell, 2007; Roberts, 2008). Geomagnetic field behaviour of paleointensity variations and excursions, topographic relief, heterogeneous magnetization distribution, and instrument noise during observation may result in short-wavelength fluctuations. High-frequency variations are significant when data collection near the magnetic source layer (e.g., near-bottom magnetic anomaly profiles). Therefore, different amplitudes of random noises are added to the magnetic anomaly profile to test the robustness of the SWCS method. In the following, the magnetic anomaly profiles (Fig. 3b) are added with ± 30 nT, ± 50 nT and ±100 nT random noises, respectively (Fig. 11a–c) to test the robustness of the SWCS method.

The identification results of marine magnetic anomaly profiles with ± 30 nT, ± 50 nT and ± 100 nT random noises are shown in Fig. 12a–c. The theoretical windows of polarity chron C27, C28 and C29 are derived from the forward modelled marine magnetic anomalies in Fig. 3b. The results show that the polarity chron C27, C28 and C29 are all correctly identified with the highest curve similarities at the corresponding sliding step 1, 3 and 5, respectively.

To investigate the detailed effects of the different amplitudes of random noise on identifying marine magnetic anomalies, we change the amplitude of random noises from 0 to 200 nT. The identification results of the polarity chron C27, C28 and C29 with different amplitudes of random noises are shown in Fig. 13a–c. The results show that the CCS is jumping and fluctuating under the effects of random noises. However, the polarity chron C27, C28 and C29 can still be correctly identified under random noises with the amplitude in the range of 0 ~ 121 nT, 0 ~ 165 nT and 0 ~ 71 nT, respectively.

Applications in actual marine magnetic anomalies

Southwest Pacific Profile

In the following, the profile EL33 of Southwest Pacific is derived from Cande (1976) to test the feasibility and effectiveness of the SWCS method. The synthetic and observed marine magnetic anomalies of EL33 are shown in Fig. 14a and b, respectively. The synthetic magnetic anomalies of EL33 are divided into six fragments, C32, C31, C30, C29, C28 and C27, as theoretical windows (Fig. 14a). Then the SWCS method is used to calculate the curve similarity between the theoretical windows and the observed marine magnetic anomalies of EL33. In the curve similarity calculation, every peak and trough of the theoretical windows and observed marine magnetic anomalies are divided into ten blocks. Figure 15a–f show the identification results of the polarity chron C32-27,

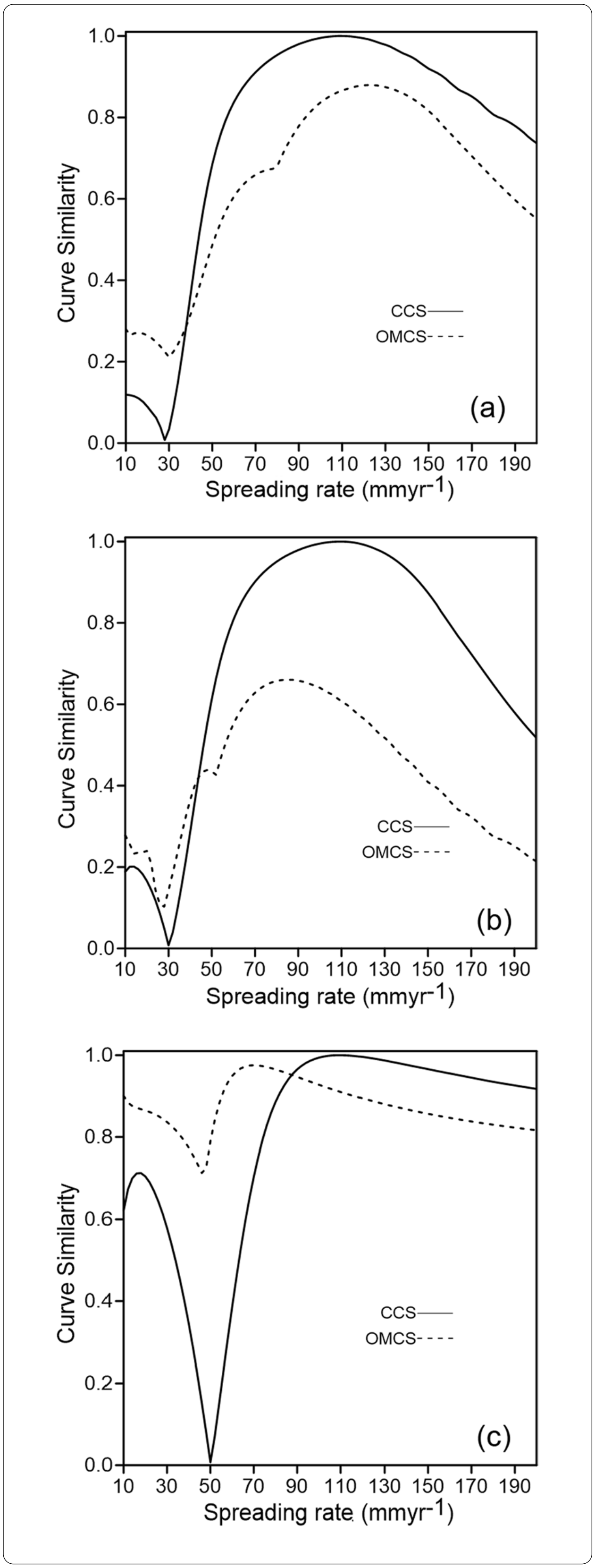

Fig. 10 The identification results of the polarity chron C27, C28 and C29 under different spreading rates. **a** The identification results of the polarity chron C27; **b** The identification results of the polarity chron C28; **c** The identification results of the polarity chron C29. The solid lines represent the curve similarity between the theoretical window and the observed magnetic anomalies at the position of the corresponding steps (CCS). The dashed lines represent the maximum absolute curve similarity values between the theoretical window and the observed magnetic anomalies at the position outside of the corresponding steps (OMCS)

respectively. The results show that a series of curve similarity values are derived as the theoretical windows slide along the observed marine magnetic anomaly profile. Figure 15a, b show that the polarity chron C32 and C31 are correctly identified with the highest curve similarity value of 0.80 and 0.54 at the corresponding step 1 and 5, respectively. The polarity chron C30 should be identified at step 7. However, the curve similarity 0.94 at step 3 is greater than the curve similarity 0.61 at step 7 (Fig. 15c); thus the polarity chron C30 is misidentified. Figure 15d shows the polarity chron C29 is correctly identified with the highest curve similarity 0.94 at the corresponding step 9. The polarity chron C28 should be identified at step 11. However, the curve similarity 0.87 at step 3 is greater than the curve similarity 0.74 at step 11 (Fig. 15e). Thus the polarity chron C28 is misidentified. Misidentification also happens for the polarity chron C27; it should be identified at step 13. However, the curve similarity 0.93 at step 9 is greater than the curve similarity 0.88 at step 13 (Fig. 15f); thus, the polarity chron C27 is also misidentified.

The magnetic anomalies of polarity chron C27, C28 and C30 are misidentified because these magnetic anomalies are only composed of one peak and one trough, and the magnetic anomalies are significantly affected by disturbances (Fig. 14b). To overcome this problem, we combined the polarity chron C31 and C30 as a theoretical window and polarity chron C27, C28 and C29 as a theoretical window, respectively. Figure 15g shows the identification results of the polarity chron C30-31. The highest curve similarity value is 0.57 at step 5, corresponding to the magnetic anomaly of polarity chron C30-31. Thus the polarity chron C30-31 is correctly identified. Figure 15h shows the identification results of the polarity chron C27-29. The highest curve similarity value is 0.86 at step 9, corresponding to the magnetic anomaly of polarity chron C27-29. Thus the polarity chron C27-29 is correctly identified. Therefore, combined polarity chrons can take advantage of comparing sequences of anomalies

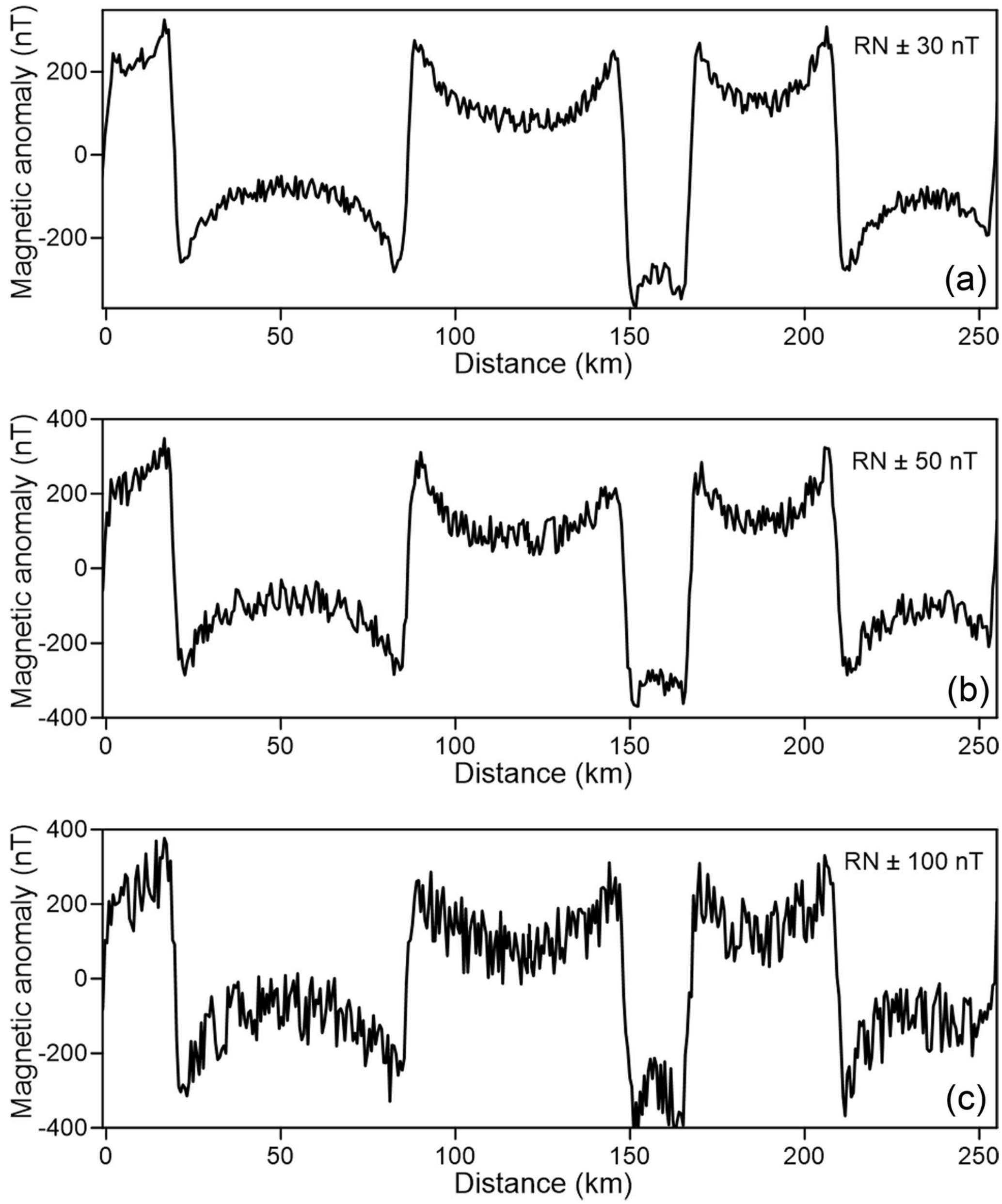

Fig. 11 The marine magnetic anomaly profiles with different amplitude of random noises. **a** Magnetic anomaly profile with ± 30 nT noises. **b** Magnetic anomaly profile with ± 50 nT noises. **c** Magnetic anomaly profile with ± 100 nT noises

and involve more feature information, thus improving the identification accuracy.

East Pacific Rise Profile

Another marine magnetic anomaly profile covering recent polarity chrons derived from Li et al. (2021) is used to test the effectiveness of the SWCS method. Figure 16 shows the synthetic and observed magnetic anomaly profile of Area 1 (Hereafter abbreviated as A1) in the East Pacific Rise. The synthetic magnetic anomalies are calculated by a magnetized oceanic crust with 0.5 km thick and 3.5 km below the sea surface and a with full spreading rate of 160 mm/yr, and the magnetization is based on absolute paleointensity studies. The observed magnetic anomalies are stacked results of different profiles in Area 1 to suppress noises (Li et al., 2021). We divided the synthetic magnetic anomalies into four sections, Brunhes,

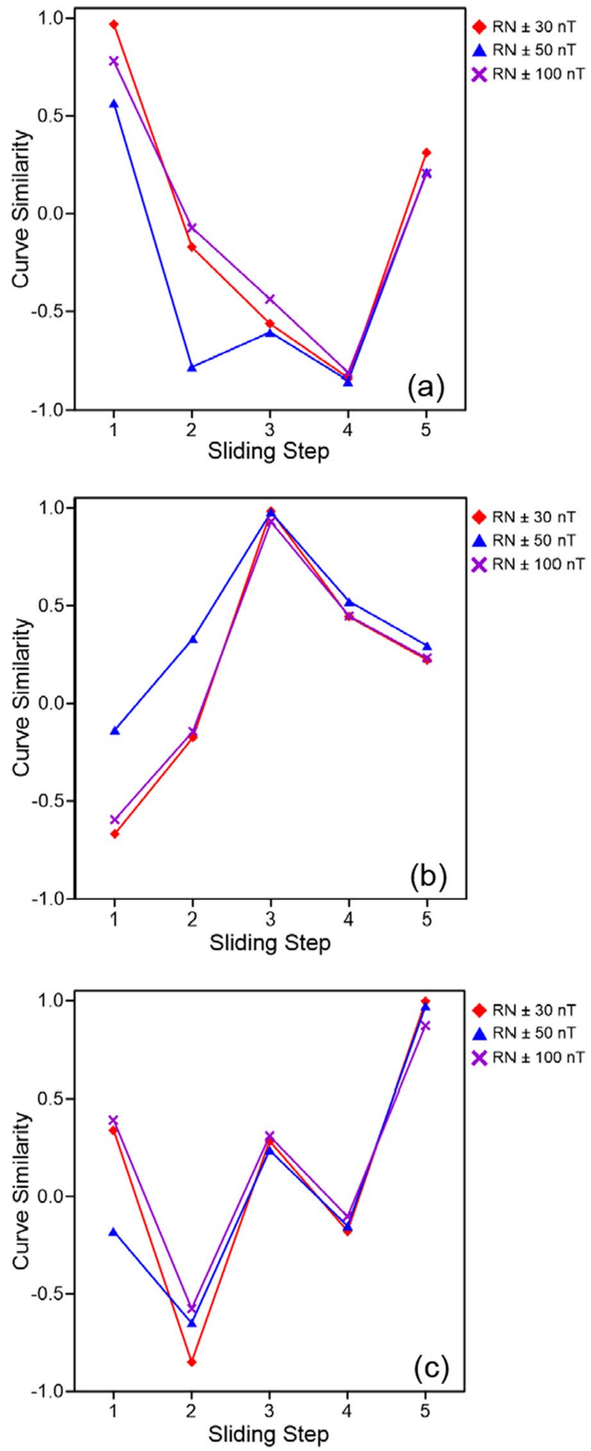

Fig. 12 Identification results of the polarity chron C27, C28 and C29 under different random noises. **a** The identification results of the polarity chron C27. **b** The identification results of the polarity chron C28. **c** The identification results of the polarity chron C29

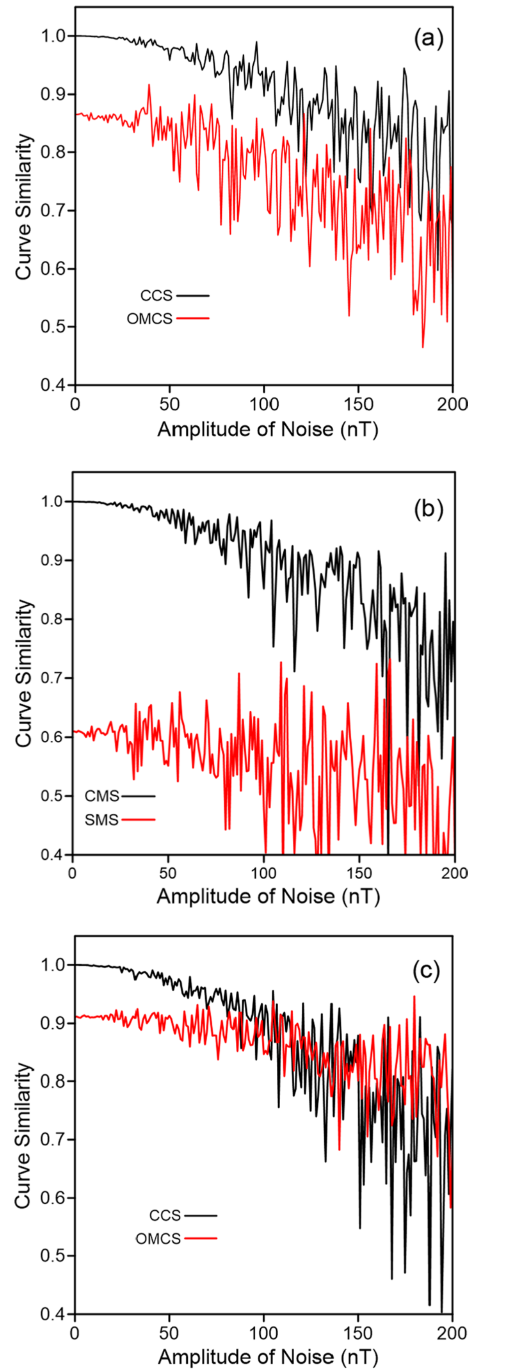

Fig. 13 The identification results of the polarity chron C27-29 with different amplitude of random noises. **a** The identification results of the polarity chron C27. **b** The identification results of the polarity chron C28. **c** The identification results of the polarity chron C29. The black lines represent the curve similarity between the theoretical window and the observed magnetic anomalies at the position of the corresponding steps (CCS). The red lines represent the maximum absolute curve similarity values between the theoretical window and the observed magnetic anomalies at the position outside of the corresponding steps (OMCS)

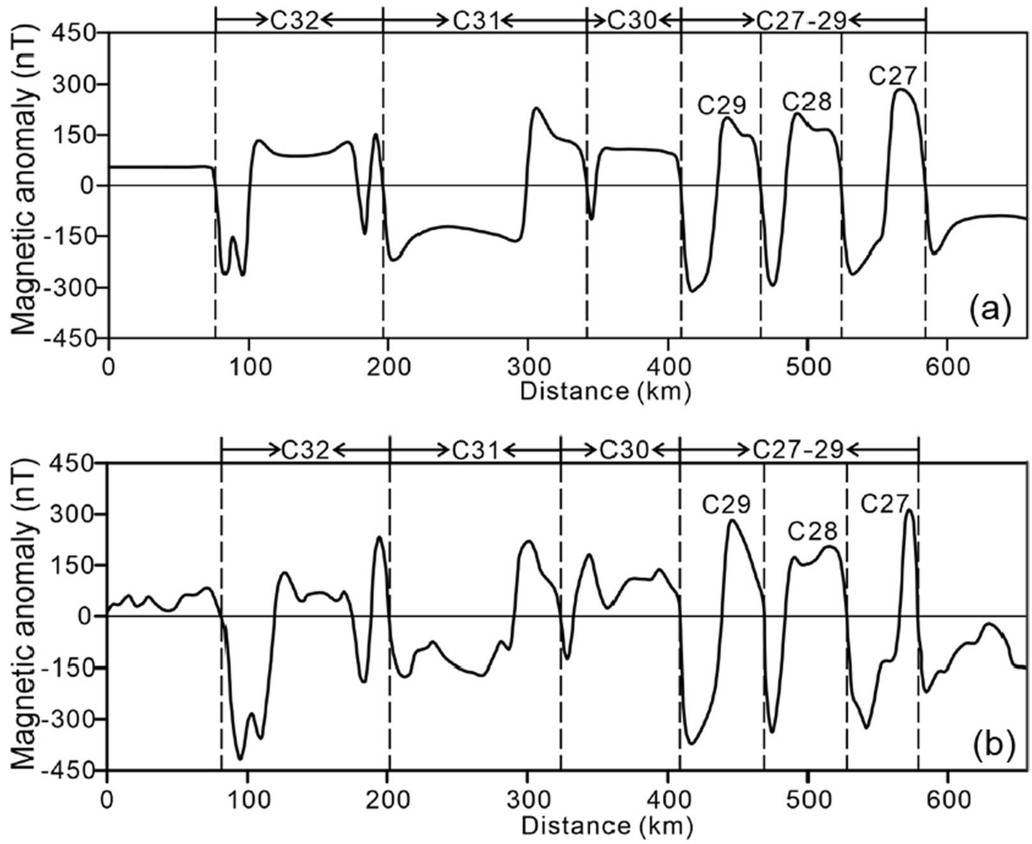

Fig. 14 The synthetic and observed marine magnetic anomalies of EL33 (From Cande 1976). **a** The synthetic marine magnetic anomalies of EL33. **b** The observed marine magnetic anomalies of EL33. Dashed lines show the boundaries of magnetic anomalies of different polarity chrons

Matuyama, Gauss and Gilbert, as theoretical windows. Then the SWCS method is used to calculate the curve similarity between the theoretical windows and the observed marine magnetic anomalies of profile A1. In the curve similarity calculation, every peak and trough of the theoretical windows and observed marine magnetic anomalies are divided into ten blocks. Short fluctuations with an age span of less than 0.1 Ma are not treated by a separately sliding step; instead, they are contained in the adjacent larger polarity chrons. Figures 17a–d show the identification results of the Brunhes, Matuyama, Gauss and Gilbert chrons, respectively. The results show that a series of curve similarity values are derived as the theoretical windows slide along the observed magnetic anomaly profile. Figure 17a shows that the Brunhes chron is correctly identified with the highest curve similarity value of 0.69 at the corresponding step 1; however, the curve similarity is -0.84 at step 3, which reflects that the short time window has low identification ability. Figure 17b shows that the Matuyama chron is correctly identified with the highest curve similarity value of 0.76 at the corresponding step 2. Figure 17c shows that the Gauss chron is correctly identified with the highest curve similarity value of 0.80 at the corresponding step 7. Figure 17d shows that the Gilbert chron is correctly identified with the highest curve similarity value of 0.81 at the corresponding step 10. The identification results provided a quantitative evaluation of the similarity between the synthetic and observed magnetic anomalies of profile A1 and verified the feasibility of the SWCS method.

Discussion

The SWCS method provides a measure to objectively identify marine magnetic anomalies and quantitatively evaluate the identification results. Synthetic model tests show that the SWCS method can identify fast-spreading magnetic anomalies; however, it has difficulty identifying slow-spreading marine magnetic anomalies. One important reason is that the signal attenuation increases as the

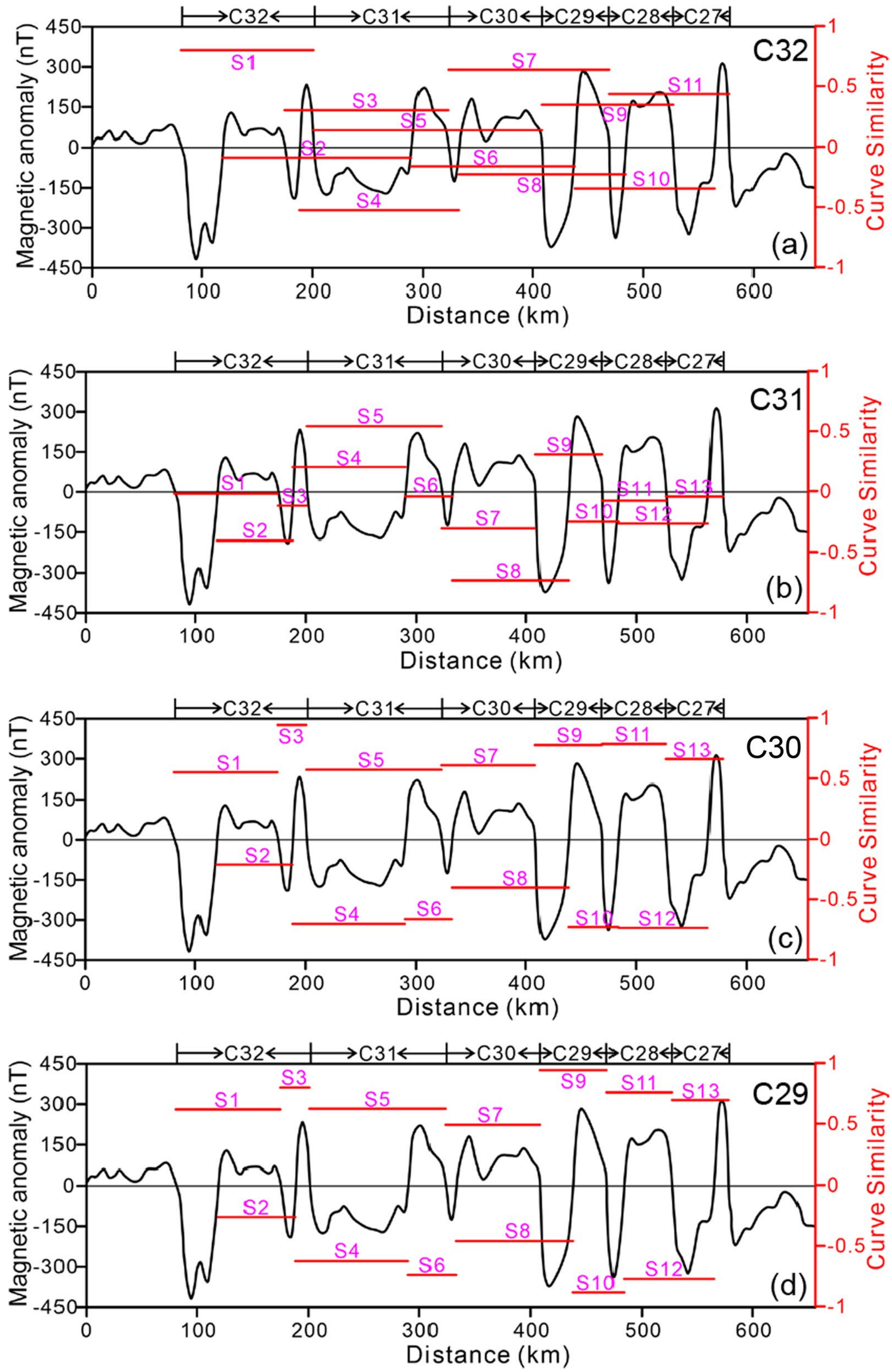

Fig. 15 The identification results of the polarity chron C32-27 of the marine magnetic profile EL33. **a**–**f** The identification results of the polarity chron C32, C31, C30, C29, C28 and C27, respectively. **g** The identification results of the polarity chron C30-31. **h** The identification results of the polarity chron C27-29. The red lines represent the values of the curve similarity in different steps (Magenta marks)

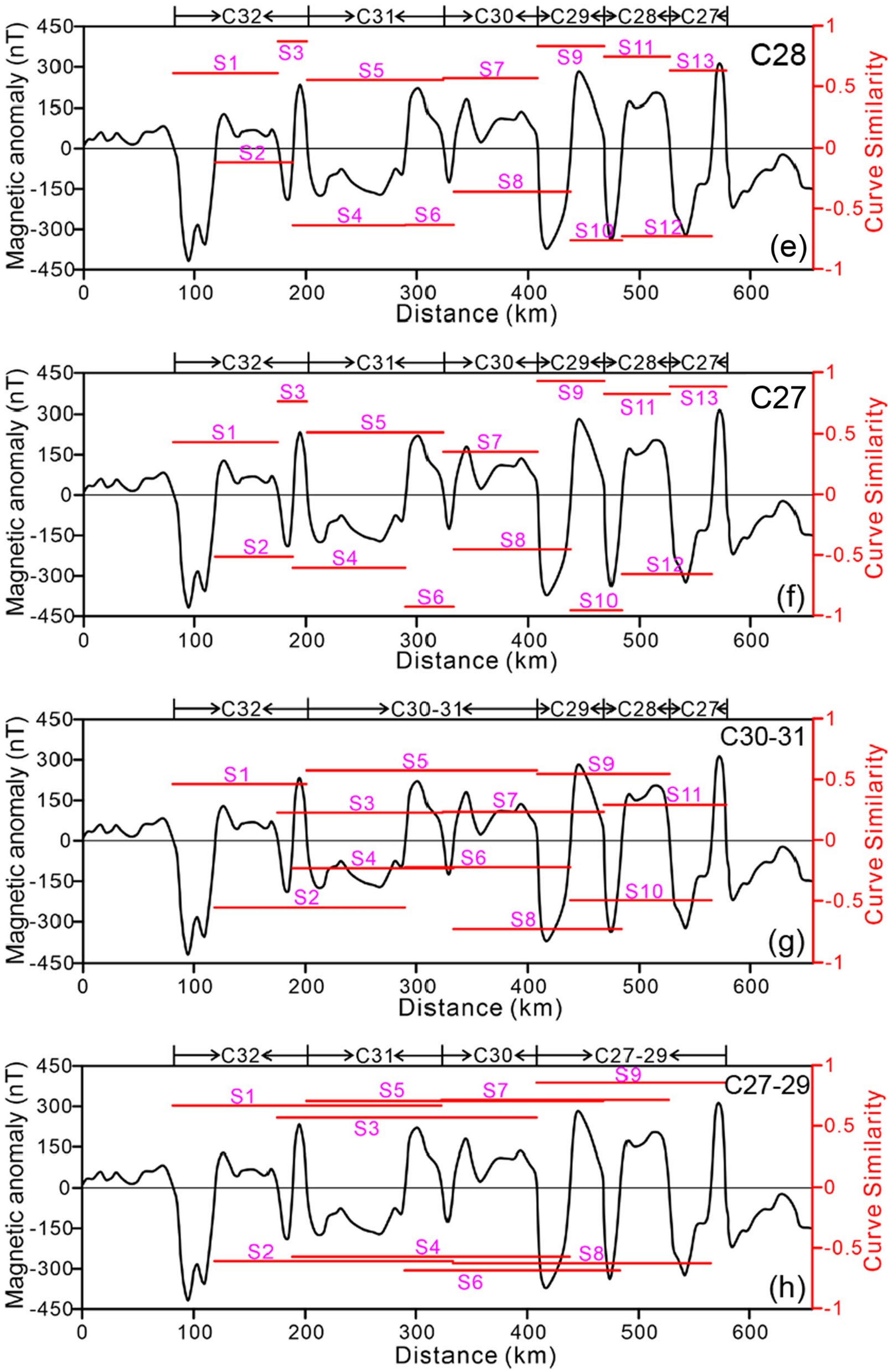

Fig. 15 continued

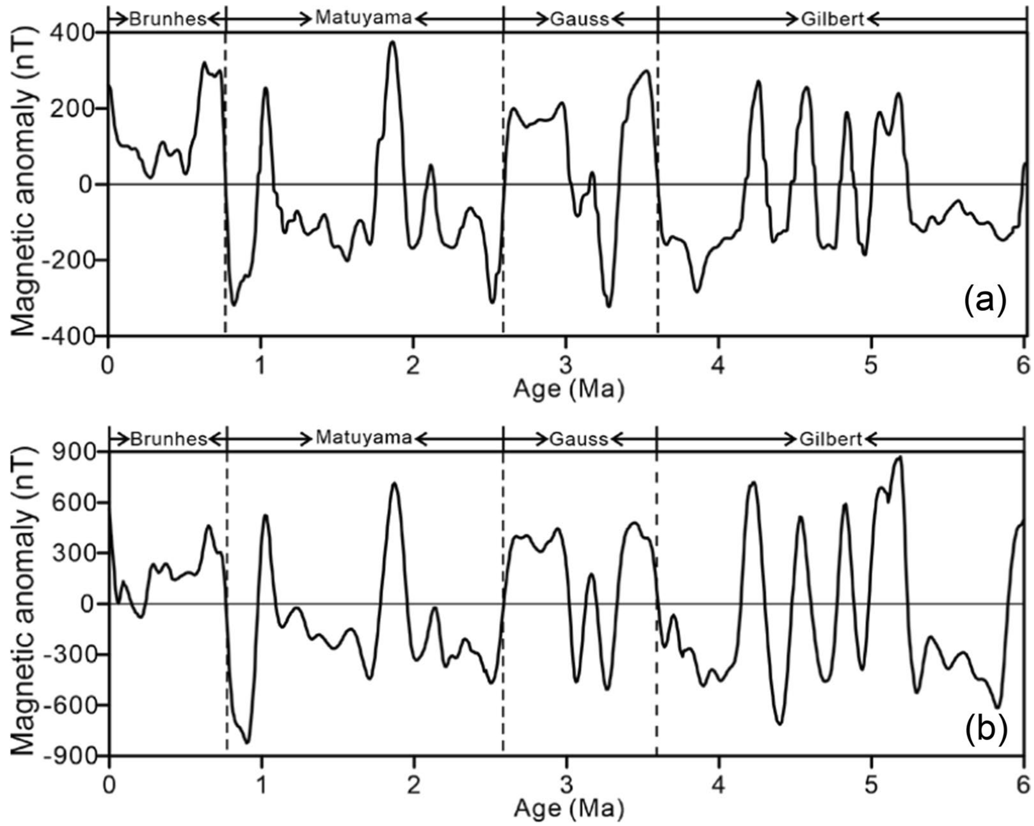

Fig. 16 The synthetic and observed marine magnetic anomalies of profile Area 1 (From Li et al., 2021). **a** The synthetic marine magnetic anomalies of profile A1. **b** The observed marine magnetic anomalies of profile A1. Dashed lines show the boundaries of magnetic anomalies of different chron sections

ratio of seafloor depth to the width of the magnetization blocks increases. Therefore, a potential measure to improve the identification of slow-spreading magnetic anomalies is to derive high-resolution magnetic data from the near-bottom magnetic observations (Honsho et al., 2009). However, the effects of alteration, deposited hydrothermal materials and small-scale geological structures will disturb the near-bottom observation. Therefore, methods of suppressing disturbances (e.g., stacked anomalies, upward continuation and low pass filtering) are suggested to process the magnetic data before identification. Furthermore, the identification of actual marine magnetic anomalies shows that magnetic anomalies of single polarity chrons or short time windows usually involve limited feature information and disturbances may significantly affect the identification results. Therefore, combined polarity chrons have advantages in constructing theoretical windows for identifying marine magnetic anomalies.

Deep-sea drilling and magnetization inversion studies show that the magnetic structure of the oceanic crust is anisotropic with changes in both vertical and horizontal directions (Wilson et al., 2006; Gee and Kent, 2007). Given the complexity of the magnetic structure of the oceanic crust, considering the detailed magnetization structure of the oceanic crust may improve the identification accuracy of the marine magnetic anomalies. However, it is beyond the scope of this study. The advantage of the SWCS method is that it can quantitatively evaluate the similarity between the synthetic and observed magnetic anomalies in any case.

Conclusion

The SWCS method is feasible and effective in identifying fast-spreading magnetic anomalies but has difficulty in identifying slow-spreading marine magnetic anomalies. Regardless of its limitation, the SWCS method can quantitatively evaluate the similarity between the synthetic and observed magnetic anomalies in any case. The applications in the actual marine magnetic anomalies show that magnetic anomalies of single polarity chrons or short time windows usually have limited feature information; In contrast, combined polarity chrons can take

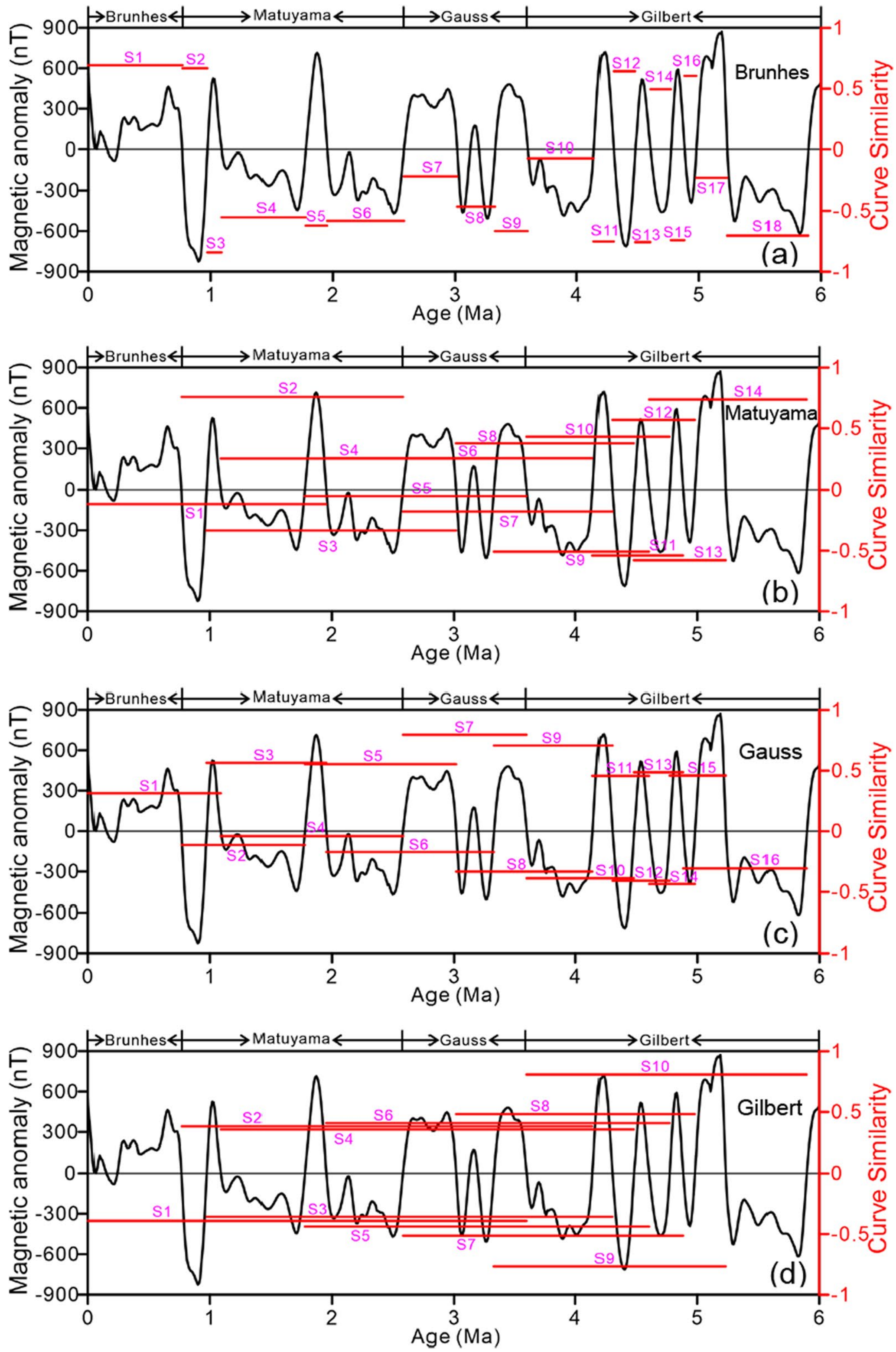

Fig. 17 The identification results of the magnetic anomalies of profile A1. **a**–**d** The identification results of the Brunhes, Matuyama, Gauss and Gilbert chrons, respectively. The red lines represent the values of the curve similarity in different steps (Magenta marks)

advantage of comparing sequences of anomalies, thus may improve the identification accuracy of marine magnetic anomalies.

Abbreviations
SWCS: Sliding window curve similarity; Ma: Million years ago; CCS: the curve similarity at the position of the corresponding steps; OMCS: the maximum absolute curve similarity outside of the corresponding steps.

Acknowledgements
We sincerely thank Jérôme Dyment and Roi Granot for their extensive reviews and suggestions that significantly improved the paper.

Author contributions
MW: conceptualization, writing and editing, funding acquisition; JC: reviewing; JL: reviewing and editing; XL: software. All authors read and approved the final manuscript.

Funding
This research was funded by the Doctoral Research Start Fund Project (Grant No. 2019jb19), Scientific Research Platform Project of Suzhou University (Grant No. 2021XJPT54) and Quality Engineering Project of Department of Education of Anhui Province (Grant No. 2021xsxxkc294). Doctoral Research Start Fund Project,2019jb19,Mingming Wang,Scientific Research Platform Project of Suzhou University,2021XJPT54,Mingming Wang,Quality Engineering Project of Department of Education of Anhui Province,2021xsxxkc294,Mingming Wang

Availability of data and materials
The data generated and analysed of the study are available from MW.

Declarations

Competing interests
The authors declare that they have no competing interests.

Author details
[1]School of Resources and Civil Engineering, Suzhou University, Suzhou 234000, China. [2]School of Earth and Space Sciences, University of Science and Technology of China, Hefei 230000, China. [3]National Engineering Research Center of Coal Mine Water Hazard Controlling, Suzhou 234000, China.

Received: 2 April 2022 Accepted: 17 May 2022
Published online: 27 May 2022

References
Blakely RJ (1976) An age-dependent, two-layer model for marine magnetic anomalies. In: Woollard GP, Sutton GH, Manghnani MH, Moberly R (eds) The geophysics of the Pacific Ocean basin and its margin. American Geophysical Union, Washington, DC. https://doi.org/10.1029/GM019p0227
Busse FH, Simitev RD (2008) Toroidal flux oscillation as possible cause of geomagnetic excursions and reversals. Phys Earth Planet Inter 168(3):237–243. https://doi.org/10.1016/j.pepi.2008.06.007
Cande SC (1976) A palaeomagnetic pole from Late Cretaceous marine magnetic anomalies in the Pacific. Geophys J Int 44(3):547–566. https://doi.org/10.1111/j.1365-246X.1976.tb00292.x
Cande SC, Kent DV (1976) Constraints imposed by the shape of marine magnetic anomalies on the magnetic source. J Geophys Res 81(23):4157–4162. https://doi.org/10.1029/JB081i023p04157
Cande SC, Kent DV (1995) Revised calibration of the geomagnetic polarity timescale for the Late Cretaceous and Cenozoic. J Geophys Res Solid Earth 100(B4):6093–6095. https://doi.org/10.1029/94JB03098
Choe H, Dyment J (2020) Fading magnetic anomalies, thermal structure and earthquakes in the Japan Trench. Geology 48(3):278–282. https://doi.org/10.1130/G46842.1
Dick HJB, Lin J, Schouten H (2003) An ultraslow-spreading class of ocean ridge. Nature 426(6965):405–412. https://doi.org/10.1038/nature02128
Dyment J, Arkani-Hamed J (1995) Spreading-rate-dependent magnetization of the oceanic lithosphere inferred from the anomalous skewness of marine magnetic anomalies. Geophys J Int 121(3):789–804. https://doi.org/10.1111/j.1365-246X.1995.tb06439.x
Dyment J, Arkani-Hamed J (1998) Contribution of lithospheric remanent magnetization to satellite magnetic anomalies over the world's oceans. J Geophys Res Solid Earth 103(B7):15423–15441. https://doi.org/10.1029/97JB03574
Dyment J, Cande SC, Arkani-Hamed J (1994) Skewness of marine magnetic anomalies created between 85 and 40 Ma in the Indian Ocean. J Geophys Res Solid Earth 99(B12):24121–24134. https://doi.org/10.1029/94jb02061
Ferré EC, Kupenko I, Martín-Hernández F et al (2021) Magnetic sources in the Earth's mantle. Nat Rev Earth Environ 2(1):59–69. https://doi.org/10.1038/s43017-020-00107-x
Gee JS, Kent DV (2007) Source of oceanic magnetic anomalies and the geomagnetic polarity timescale. Treatise Geophysics 5:455–507. https://doi.org/10.1016/B978-044452748-6.00097-3
Gee JS, Cande SC, Hildebrand JA et al (2000) Geomagnetic intensity variations over the past 780 kyr obtained from near-seafloor magnetic anomalies. Nature 408(6814):827–832
Granot R, Dyment J (2015) The cretaceous opening of the South Atlantic Ocean. Earth & Planet Sci Lett 414:156–163. https://doi.org/10.1016/j.epsl.2015.01.015
Granot R, Dyment J (2019) The influence of post-accretion sedimentation on marine magnetic anomalies. Geophys Res Lett 46(9):4645–4652. https://doi.org/10.1029/2019GL082265
Gürer D, Granot R, van Hinsbergen DJJ (2022) Plate tectonic chain reaction revealed by noise in the Cretaceous quiet zone. Nat Geosci. https://doi.org/10.1038/s41561-022-00893-7
Harrison CGA (1987) Marine magnetic anomalies-the origin of the stripes. Annu Rev Earth Planet Sci 15(1):505–543. https://doi.org/10.1146/annurev.ea.15.050187.002445
Honsho C, Dyment J, Tamaki K et al (2009) Magnetic structure of a slow-spreading ridge segment: Insights from near-bottom magnetic measurements on board a submersible. J Geophys Res Solid Earth. https://doi.org/10.1029/2008JB005915
Jacob J, Dyment J, Yatheesh V (2014) Revisiting the structure, age, and evolution of the Wharton Basin to better understand subduction under Indonesia. J Geophys Res Solid Earth 119(1):169–190. https://doi.org/10.1002/2013JB010285
Kidd RGW (1977) The nature and shape of the sources of marine magnetic anomalies. Earth & Planet Sci Lett 33(3):310–320. https://doi.org/10.1016/0012-821X(77)90083-8
Korenaga J (1995) Comprehensive analysis of marine magnetic vector anomalies. J Geophys Res Solid Earth 100(B1):365–378. https://doi.org/10.1029/94JB02596
Laj C, Channell JET (2007) Geomagnetic excursions, in treatise on geophysics. In: Kono M (ed) Geomagnetism. Elsevier, Amsterdam, pp 373–416
Li CF, Xu X, Lin J et al (2014) Ages and magnetic structures of the South China Sea constrained by deep tow magnetic surveys and IODP Expedition 349. Geochem Geophys Geosystems 15(12):4958–4983. https://doi.org/10.1002/2014GC005567
Li YJ, Liu QS, Wei DP et al (2018) Variations of Earth Magnetic Field Intensity for the Past 5 Myr Derived From Marine Magnetic Anomalies in a Slow-to-intermediate-spreading South Atlantic Ridge. J Geophys Res Solid Earth 123(9):7321–7337. https://doi.org/10.1029/2018JB016099
Li YJ, Liu JB, Liu QS (2021) Geomagnetic field paleointensity spanning the past 11 Myr from Marine Magnetic Anomalies in the ssouthern hemisphere. Geophys Res Lett 48(11):e2021GL093235. https://doi.org/10.1029/2021GL093235
Lonsdale P (1977) Structural geomorphology of a fast-spreading rise crest: the East Pacific Rise near 3° 25′ S. Mar Geophys Res 3(3):251–293. https://doi.org/10.1007/BF00285656
Macdonald KC (1982) Mid-ocean ridges: Fine scale tectonic, volcanic and hydrothermal processes within the plate boundary zone. Annu Rev Earth Planet Sci 10(1):155–190. https://doi.org/10.1146/annurev.ea.10.050182.001103
Menard HW (1967) Sea floor spreading, topography, and the second layer. Science 157(3791):923–924. https://doi.org/10.1126/science.157.3791.923

Müller RD, Sdrolias M, Gaina C, Roest RW (2008) Age, spreading rates, and spreading asymmetry of the world's ocean crust. Geochem Geophys Geosyst 9(4):1–16. https://doi.org/10.1029/2007GC001743
Roberts AP (2008) Geomagnetic excursions: knowns and unknowns. Geophys Res Lett 35(17):1–7. https://doi.org/10.1029/2008GL034719
Roberts AP, Lewin-Harris JC (2000) Marine magnetic anomalies: evidence that 'tiny wiggles' represent short-period geomagnetic polarity intervals. Earth Planet Sci Lett 183(3–4):375–388. https://doi.org/10.1016/S0012-821X(00)00290-9
Talwani M (1964) (1964) Computation of magnetic anomalies caused by two-dimensional bodies of arbitrary shape. Computers in the Mineral Industries 1:464–480
Tominaga M, Tivey MA, Sager WW (2021) A new middle to Late Jurassic Geomagnetic Polarity Time Scale (GPTS) from a multiscale marine magnetic anomaly survey of the Pacific Jurassic Quiet Zone. J Geophys Res Solid Earth 126(3):e2020JB021136. https://doi.org/10.1029/2020JB021136
Veevers JJ, Li ZX (1991) Review of seafloor spreading around Australia. II. Marine magnetic anomaly modelling. Aus J Earth Sci 38(4):391–408. https://doi.org/10.1080/08120099108727980
Vine FJ (1966) Spreading of the Ocean Floor: New Evidence: Magnetic anomalies may record histories of the ocean basins and Earth's magnetic field for 2×10^8 years. Science 154(3755):1405–1415. https://doi.org/10.1126/science.154.3755.1405
Vine FJ, Matthews DH (1963) Magnetic anomalies over oceanic ridges. Nature 199:947–949. https://doi.org/10.1038/199947a0
Wang MM, Liu ZX (2018) The effects of anisotropy of marine magnetic anomalies on the Curie point depth estimates from spectral analysis. Acta Geophys 66(5):1019–1030. https://doi.org/10.1007/s11600-018-0197-z
Wilson DS, Teagle DAH, Alt JC et al (2006) Drilling to gabbro in intact ocean crust. Science 312(5776):1016–1020. https://doi.org/10.1126/science.1126090
Won IJ, Bevis M (1987) Computing the gravitational and magnetic anomalies due to a polygon: algorithms and fortran subroutines. Geophysics 52(2):202–205. https://doi.org/10.1190/1.1442298

Publisher's Note